AFRL-ML-WP-TP-2004-401

MICROMECHANICAL ANALYSIS OF THREE-DIMENSIONAL OPEN-CELL FOAMS USING THE MATRIX METHOD FOR SPACE FRAME STRUCTURES

A.K. Roy

Mechanics Section (AFRL/MLBCM), Structural Materials Branch
Nonmetallic Materials Division
Materials and Manufacturing Directorate
Air Force Research Laboratory, Air Force Materiel Command
Wright-Patterson AFB, OH 45433-7750

K. Li and X.-L. Gao
Michigan Technological University

NOVEMBER 2004

Approved for public release; distribution is unlimited.

STINFO FINAL REPORT

MATERIALS AND MANUFACTURING DIRECTORATE
AIR FORCE RESEARCH LABORATORY
AIR FORCE MATERIEL COMMAND
WRIGHT-PATTERSON AIR FORCE BASE, OH 45433-7750

NOTICE

Using government drawings, specifications, or other data included in this document for any purpose other than government procurement does not in any way obligate the U.S. Government. The fact that the government formulated or supplied the drawings, specifications, or other data does not license the holder or any other person or corporation; or convey any rights or permission to manufacture, use, or sell any patented invention that may relate to them.

This report has been reviewed by the AFRL Wright Site Office of Public Affairs (WS/PA) and is releasable to the National Technical Information Service (NTIS). At NTIS, it will be available to the general public, including foreign nationals.

This technical report has been reviewed and is approved for publication.

//s//

Pamela M. Schaefer
Principal Materials Engineer
Technical & Strategic Planning Office
Materials and Manufacturing Directorate

Copies of this report should not be returned unless return is required by security considerations, contractual obligations, or notice on a specific document.

REPORT DOCUMENTATION PAGE

Form Approved
OMB No. 0704-0188

1. REPORT DATE *(DD-MM-YY)*	2. REPORT TYPE	3. DATES COVERED *(From - To)*
November 2004	Conference paper preprint	

4. TITLE AND SUBTITLE

MICROMECHANICAL ANALYSIS OF THREE-DIMENSIONAL OPEN-CELL FOAMS USING THE MATRIX METHOD FOR SPACE FRAME STRUCTURES

5a. CONTRACT NUMBER
IN-HOUSE

5b. GRANT NUMBER

5c. PROGRAM ELEMENT NUMBER
N/A

6. AUTHOR(S)

A.K. Roy (Mechanics Section (AFRL/MLBCM), Structural Materials Branch)
K. Li and X.-L. Gao (Michigan Technological University)

5d. PROJECT NUMBER
M03R

5e. TASK NUMBER
10

5f. WORK UNIT NUMBER
00

7. PERFORMING ORGANIZATION NAME(S) AND ADDRESS(ES)

Mechanics Section (AFRL/MLBCM), Structural Materials Branch
Nonmetallic Materials Division
Materials and Manufacturing Directorate
Air Force Research Laboratory, Air Force Materiel Command
Wright-Patterson Air Force Base, OH 45433-7750

Michigan Technological University

8. PERFORMING ORGANIZATION REPORT NUMBER

AFRL-ML-WP-TP-2004-401

9. SPONSORING/MONITORING AGENCY NAME(S) AND ADDRESS(ES)

Materials and Manufacturing Directorate
Air Force Research Laboratory
Air Force Materiel Command
Wright-Patterson Air Force Base, OH 45433-7750

10. SPONSORING/MONITORING AGENCY ACRONYM(S)
AFRL/MLBCM

11. SPONSORING/MONITORING AGENCY REPORT NUMBER(S)
AFRL-ML-WP-TP-2004-401

12. DISTRIBUTION/AVAILABILITY STATEMENT
Approved for public release; distribution is unlimited.

13. SUPPLEMENTARY NOTES

This work has been submitted to the Society of Manufacturing Engineers (SME) for publication in the 14th International Conference on Composite Materials (ICCM-14). One of the authors is a U.S. Government employee; therefore, the U.S. Government is joint owner of the work. If published, SME may assert copyright. If so, the United States has for itself and other acting on its behalf and unlimited, paid-up, nonexclusive, irrevocable worldwide license. Any other form of use is subject to copyright restrictions.

ABSTRACT ***(Maximum 200 Words), ,***

A micromechanical model for three-dimensional open-cell foams is developed by using the matrix method for space frames in structural mechanics and tetrakaidcahedral unit cells. The effective elastic properties of foams are determined employing unit cells subjected to three different modes of loading. The thirty-six struts of each tetrakaidecahedral unit cell are treated as uniform slender beams, and the twenty-four vertices as rigid joints. All four-deformation mechanisms (i.e., stretching, shearing, bending and twisting) possible under the specified loadings are incorporated, and four different strut cross section shapes (i.e., circle, square, equilateral triangle and Plateau border) are treated in a unified manner. The formulas for determining the effective Young's modulus, Poisson's ratio and shear modulus of open-cell foams that are undergoing linearly elastic deformations are derived using the composite homogentization theory. The new formulas include all necessary parameters, unlike those provided by existing models.

15. SUBJECT TERMS

Micromechanics, Open-cell foams, Effective elastic properties, Matrix method, Composite homogenization theory

16. SECURITY CLASSIFICATION OF:			17. LIMITATION OF ABSTRACT:	18. NUMBER OF PAGES	19a. NAME OF RESPONSIBLE PERSON (Monitor)
a. REPORT	b. ABSTRACT	c. THIS PAGE			Ajit K. Roy
Unclassified	Unclassified	Unclassified	SAR	18	19b. TELEPHONE NUMBER *(Include Area Code)* (937) 255-9034

Standard Form 298 (Rev. 8-98)
Prescribed by ANSI Std. Z39-18

MICROMECHANICAL ANALYSIS OF THREE-DIMENSIONAL OPEN-CELL FOAMS USING THE MATRIX METHOD FOR SPACE FRAME STRUCTURES

K. Li and **X.-L. Gao***

Department of Mechanical Engineering – Engineering Mechanics, Michigan Technological University, 1400 Townsend Drive, Houghton, MI 49931-1295

A. K. Roy

Materials and Manufacturing Directorate, Air Force Research Laboratory, AFRL/MLBC, Wright-Patterson Air Force Base, OH 45433-7750

ABASTRACT

A micromechanical model for three-dimensional open-cell foams is developed by using the matrix method for space frames in structural mechanics and tetrakaidecahedral unit cells. The effective elastic properties of foams are determined employing unit cells subjected to three different modes of loading. The thirty-six struts of each tetrakaidecahedral unit cell are treated as uniform slender beams, and the twenty-four vertices as rigid joints. All four deformation mechanisms (i.e., stretching, shearing, bending and twisting) possible under the specified loadings are incorporated, and four different strut cross section shapes (i.e., circle, square, equilateral triangle and Plateau border) are treated in a unified manner. The formulas for determining the effective Young's modulus, Poisson's ratio and shear modulus of open-cell foams that are undergoing linearly elastic deformations are derived using the composite homogenization theory. The new formulas include all necessary parameters, unlike those provided by existing models. These formulas indicate that the foam elastic properties depend on the relative foam density, the shape and size of the strut cross section, and the Young's modulus and Poisson's ratio of the strut material. By applying the new model, a parametric study of sample cases is conducted for carbon foams, whose modeling motivated this study. The predicted values of the effective properties agree favorably with those based on existing models and experimental data for the Mode I loading case, which is the only case that has been well studied in the literature. Comparisons of the effective elastic properties for the three loading cases quantitatively show that carbon foams exhibit certain degree of anisotropy.

KEYWORDS: Micromechanics; Open-cell foams; Effective elastic properties; Matrix method; Composite homogenization theory

1. INTRODUCTION

Microcellular graphitic carbon foams first developed at the Air Force Research Laboratory (AFRL) in 1990s (e.g., Hall and Hager, 1996) are rapidly emerging as a new class of ultra-light cellular materials for structural and thermal management applications because of their excellent mechanical and thermal properties (Roy et al., 1998). Reliable structural applications of these carbon foams depend on accurate understanding of their mechanical behavior. Carbon foams, like other cellular solids, are topology-sensitive and, therefore, their mechanical modeling requires the incorporation of cell's microstructural features.

AFRL graphitic carbon foams are blown from anisotropic pitch through a bubble forming process (e.g., Anderson et al., 2000), and, as a result, microstructures of the solidified carbon foams are controlled by the principle of minimum surface energy. As shown in Fig. 1, the microstructure of an AFRL carbon foam has a three-dimensional (3-D) open-cell topology. As a first approximation, a regular tetrakaidecahedron (see Fig. 2(a)) can be adopted as the repeating unit to represent this foam

* Corresponding author. Tel: (906)487-1898; Fax: (906)487-2822; E-mail: xgao@mtu.edu.

microstructure. Tetrakaidecahedron is known to be the only polyhedron that can pack with identical units to fill space and nearly minimize the surface energy (e.g., Weaire and Fortes, 1994). With all of its vertices connected by struts and each vertex shared by four struts, such a fourteen-sided polyhedron can be generated by uniformly truncating the six corners of an octahedron and contains eight regular hexagonal faces and six square faces.

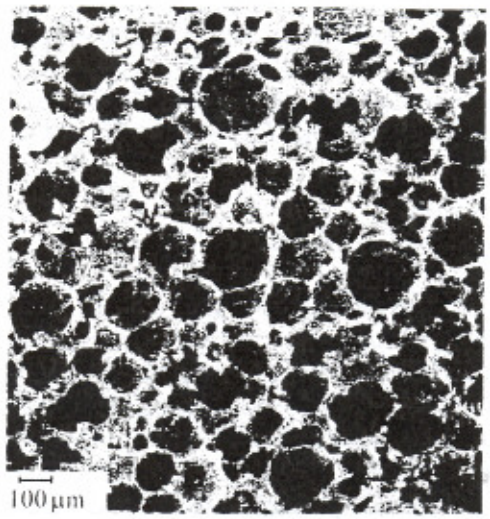

Fig. 1. Micrograph of an AFRL carbon foam (Roy et al., 1998).

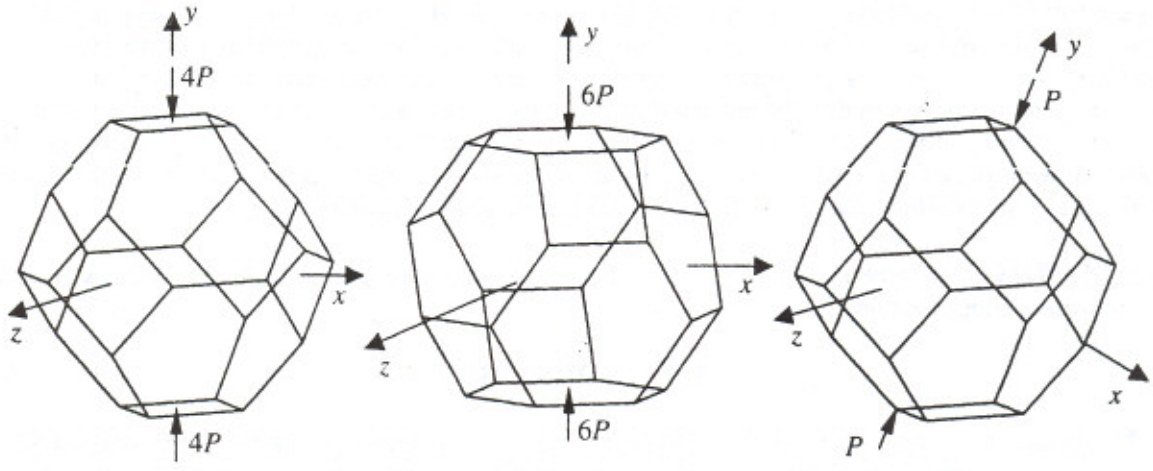

Fig. 2. Tetrakaidecahedral unit cell under loading: (a) Mode I, (b) Mode II, (c) Mode III.

Several micromechanical models for 3-D open-cell foams have been developed utilizing tetrakaidecahedral unit cells, which are reviewed in Li et al. (2003). Very recently, a micromechanics model for predicting effective Young's modulus and Poisson's ratio of such foams was provided by Li et al. (2003) using an energy method based on Castigliano's second theorem, whose predictions compare favorably with those based on available experimental data and finite element analyses. However, only Mode I loading (see Fig. 2) was considered there, as was the case with almost all previous studies on the

topic. Also, how to predict effective shear modulus was not addressed in Li et al. (2003). When loads are not applied on two opposite square faces of a tetrakaidecahedral cell, the elastic properties obtained might be different from those when the cell is subjected to Mode I loading. For example, cubic symmetry is present under Mode I loading, but is absent under Mode II or III loading. For the latter cases, anisotropy involved can be significant. Hence, new micromechanical models capable of accounting for the differences in mechanical behavior of foams (cells) under three distinct modes of loading are necessitated.

The objective of this paper is to present such a new model. The tetrakaidecahedral unit cells illustrated in Fig. 2 are adopted, and the matrix method for space frame structures and the homogenization theory for composite materials are employed in the formulation.

2. MATRIX METHOD FOR SPACE FRAME STRUCTURES

2.1 Method

In this matrix method the members of a space frame structure are regarded as rigidly connected at joints (or nodes), each of which has six degrees of freedom – three translational and three rotational – when unrestrained. The twelve possible displacements of the two joints of a member may be described relative to the (global) reference axes x, y and z or to the (local) member-oriented axes x_M, y_M and z_M, as shown in Fig. 3. The x_M axis is set to be along the axis of the member from i to j, and the y_M and z_M axes are chosen as the principal axes of the cross section at joint i of the member.

In terms of the member coordinates $\{x_M, y_M, z_M,\}$, the forces at the ends of a member are related to the displacements at the ends by the member stiffness matrix, i.e.,

$$\begin{Bmatrix} \mathbf{f}_{ij} \\ \mathbf{f}_{ji} \end{Bmatrix} = \left[\begin{array}{c:c} \mathbf{k}_{ii}^{j} & \mathbf{k}_{ij} \\ \hdashline \mathbf{k}_{ji} & \mathbf{k}_{jj}^{i} \end{array}\right] \begin{Bmatrix} \boldsymbol{\delta}_{ij} \\ \boldsymbol{\delta}_{ji} \end{Bmatrix}, \tag{1}$$

where δ_{ij} and δ_{ji} are, respectively, displacement vectors at nodes i and j, and $\mathbf{f}_{ij}$ and $\mathbf{f}_{ji}$, respectively, force vectors at nodes i and j for member "i, j". The member stiffness matrix in Eq. (1) is composed of four submatrices $\mathbf{k}_{ii}^{j}$, $\mathbf{k}_{ij}$, $\mathbf{k}_{ji}$ and $\mathbf{k}_{jj}^{i}$. The first subscript of each submatrix represents the forces arising at the end associated with this subscript caused by unit displacements occurring at the other end (associated with the second subscript).

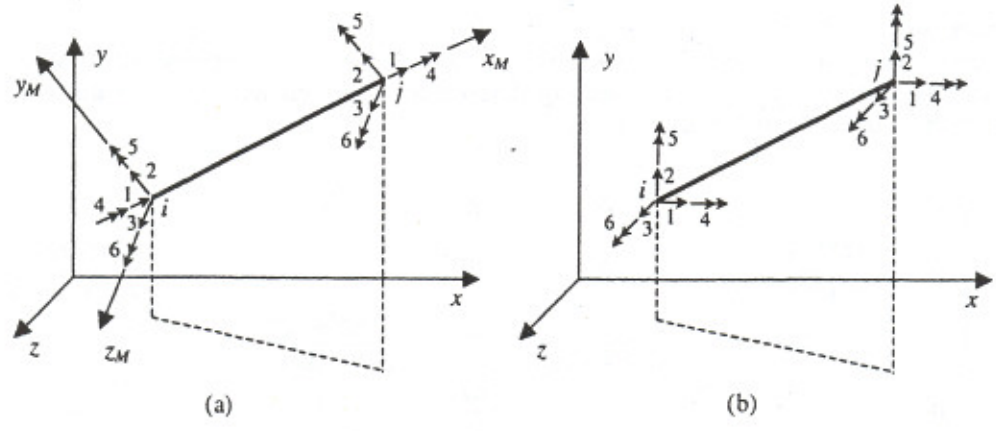

Fig. 3. Numbering system for a space frame member.

When expressed in terms of the reference coordinates $\{x, y, z\}$, Eq. (1) becomes

$$\begin{Bmatrix} \mathbf{F}_{ij} \\ \mathbf{F}_{ji} \end{Bmatrix} = \left[\begin{array}{c:c} \mathbf{K}_{ii}^{j} & \mathbf{K}_{ij} \\ \hdashline \mathbf{K}_{ji} & \mathbf{K}_{jj}^{i} \end{array}\right] \begin{Bmatrix} \boldsymbol{\Delta}_{i} \\ \boldsymbol{\Delta}_{j} \end{Bmatrix}, \tag{2}$$

where $\mathbf{F}_{ij}$ and $\mathbf{F}_{ji}$ are, respectively, force vectors at nodes i and j, Δ_i and Δ_j are, respectively, displacement vectors at nodes i and j, and

$$\mathbf{K}_{ii}^{j} = \mathbf{T}_{ij}^{-1}\mathbf{k}_{ii}^{j}\mathbf{T}_{ij},\ \mathbf{K}_{ij} = \mathbf{T}_{ij}^{-1}\mathbf{k}_{ij}\mathbf{T}_{ij},\ \mathbf{K}_{ji} = \mathbf{T}_{ij}^{-1}\mathbf{k}_{ji}\mathbf{T}_{ij},\ \mathbf{K}_{jj}^{i} = \mathbf{T}_{ij}^{-1}\mathbf{k}_{jj}^{i}\mathbf{T}_{ij}, \tag{3a–d}$$

are the global stiffness submatrices, with $\mathbf{T}_{ij}$ being the transformation matrix for member "i, j" (from global to local).

Nodal equilibrium requires that the applied loads at a node be balanced by the internal member end forces. Suppose that members "i, a", "i, b", ..., "i, n" are connected to node i. Then, the equilibrium of node i requires

$$\mathbf{P}_i = \mathbf{F}_{ia} + \mathbf{F}_{ib} + \cdots + \mathbf{F}_{in}, \tag{4}$$

where $\mathbf{P}_i$ is the applied load vector at node i. Using Eq. (2) in Eq. (4) gives

$$\mathbf{P}_i = \mathbf{K}_{ii}\Delta_i + \mathbf{K}_{ia}\Delta_a + \mathbf{K}_{ib}\Delta_b + \cdots + \mathbf{K}_{in}\Delta_n, \tag{5}$$

where $\mathbf{K}_{ii} = \mathbf{K}_{ii}^{a} + \mathbf{K}_{ii}^{b} + \cdots + \mathbf{K}_{ii}^{n}$. Subsequently, enforcing the equilibrium of all nodes results in

$$\begin{Bmatrix} \mathbf{P}_1 \\ \mathbf{P}_2 \\ \vdots \\ \mathbf{P}_N \end{Bmatrix} = \begin{bmatrix} \mathbf{K}_{11} & \mathbf{K}_{12} & \cdots & \mathbf{K}_{1N} \\ \mathbf{K}_{21} & \mathbf{K}_{22} & \cdots & \mathbf{K}_{2N} \\ \vdots & \vdots & & \vdots \\ \mathbf{K}_{N1} & \mathbf{K}_{N2} & \cdots & \mathbf{K}_{NN} \end{bmatrix} \begin{Bmatrix} \Delta_1 \\ \Delta_2 \\ \vdots \\ \Delta_N \end{Bmatrix}. \tag{6}$$

In Eq. (6), which is called the initial stiffness equation, each nodal force/displacement vector has six components. The coefficient matrix of these equations, denoted as $\mathbf{K}_I$, is known as the initial structure stiffness matrix. Each submatrix of $\mathbf{K}_I$ is a 6×6 square matrix. Equation (6) can be rearranged as

$$\left\{\begin{array}{c} \mathbf{P}_F \\ \hdashline \mathbf{P}_R \end{array}\right\} = \left[\begin{array}{c:c} \mathbf{K}_{FF} & \mathbf{K}_{FR} \\ \hdashline \mathbf{K}_{RF} & \mathbf{K}_{RR} \end{array}\right] \left\{\begin{array}{c} \Delta_F \\ \hdashline \Delta_R \end{array}\right\}, \tag{7}$$

where the subscripts **F** and **R** refer to free and restrained displacements, respectively. From Eq. (7) the free nodal displacements can then be obtained as

$$\Delta_F = \mathbf{K}_{FF}^{-1}\mathbf{P}_F. \tag{8}$$

2.2 Member Stiffness Matrix

By following the procedure used in Spillers (1972) for 2-D frames, the member stiffness submatrices for 3-D frames undergoing transverse shearing deformations as well as axial, flexural and torsional deformations are obtained, for the first time, as

$$\left(\mathbf{k}_{ii}^{j}\right)_m = \begin{bmatrix} \frac{EA}{L} & 0 & 0 & 0 & 0 & 0 \\ 0 & \frac{12AEGI_z k_y}{12EI_z L + AGk_y L^3} & 0 & 0 & 0 & \frac{6AEGI_z k_y}{12EI_z + AGk_y L^2} \\ 0 & 0 & \frac{12AEGI_y k_z}{12EI_y L + AGk_z L^3} & 0 & \frac{-6AEGI_y k_z}{12EI_y + AGk_z L^2} & 0 \\ 0 & 0 & 0 & \frac{GJ}{L} & 0 & 0 \\ 0 & 0 & \frac{-6AEGI_y k_z}{12EI_y + AGk_z L^2} & 0 & \frac{4EI_y\left(3EI_y + AGk_z L^2\right)}{12EI_y L + AGk_z L^3} & 0 \\ 0 & \frac{6AEGI_z k_y}{12EI_z + AGk_y L^2} & 0 & 0 & 0 & \frac{4EI_z\left(3EI_z + AGk_y L^2\right)}{12EI_z L + AGk_y L^3} \end{bmatrix}.$$

$$(\mathbf{k}_{ij})_m = \begin{bmatrix} -\frac{EA}{L} & 0 & 0 & 0 & 0 & 0 \\ 0 & \frac{-12AEGI_z k_y}{12EI_z L + AGk_y L^3} & 0 & 0 & 0 & \frac{6AEGI_z k_y}{12EI_z + AGk_y L^2} \\ 0 & 0 & \frac{-12AEGI_y k_z}{12EI_y L + AGk_z L^3} & 0 & \frac{-6AEGI_y k_z}{12EI_y + AGk_z L^2} & 0 \\ 0 & 0 & 0 & -\frac{GJ}{L} & 0 & 0 \\ 0 & 0 & \frac{6AEGI_y k_z}{12EI_y + AGk_z L^2} & 0 & \frac{-2EI_y(6EI_y - AGk_z L^2)}{12EI_y L + AGk_z L^3} & 0 \\ 0 & \frac{-6AEGI_z k_y}{12EI_z + AGk_y L^2} & 0 & 0 & 0 & \frac{-2EI_z(6EI_z - AGk_y L^2)}{12EI_z L + AGk_y L^3} \end{bmatrix},$$

$$(\mathbf{k}_{ji})_m = (\mathbf{k}_{ij})_m^{\mathrm{T}},$$

$$(\mathbf{k}_{ij}^{1})_m = \begin{bmatrix} \frac{EA}{L} & 0 & 0 & 0 & 0 & 0 \\ 0 & \frac{12AEGI_z k_y}{12EI_z L + AGk_y L^3} & 0 & 0 & 0 & \frac{-6AEGI_z k_y}{12EI_z + AGk_y L^2} \\ 0 & 0 & \frac{12AEGI_y k_z}{12EI_y L + AGk_z L^3} & 0 & \frac{6AEGI_y k_z}{12EI_y + AGk_z L^2} & 0 \\ 0 & 0 & 0 & \frac{GJ}{L} & 0 & 0 \\ 0 & 0 & \frac{6AEGI_y k_z}{12EI_y + AGk_z L^2} & 0 & \frac{4EI_y(3EI_y + AGk_z L^2)}{12EI_y L + AGk_z L^3} & 0 \\ 0 & \frac{-6AEGI_z k_y}{12EI_z + AGk_y L^2} & 0 & 0 & 0 & \frac{4EI_z(3EI_z + AGk_y L^2)}{12EI_z L + AGk_y L^3} \end{bmatrix}, \quad \textbf{(9a–d)}$$

where A, L are, respectively, the cross-sectional area and length of the member, I_y and I_z are the second moments of area of the member cross section, J is the polar second moment of area, E and G are, respectively, the Young's modulus and shear modulus of the member material, and k_y and k_z are the transverse shear factors. It is noted that when k_y and k_z approach infinity, Eqs. (9a–d) will be reduced to the member stiffness submatrices for members involving only axial, flexural and torsional deformations (e.g., Balfour, 1986). Substituting Eqs. (9a–d) for the member stiffness submatrices into Eqs. (3a–d) results in the following global stiffness submatrices:

$$(\mathbf{K}_{ii}^{1})_m = \mathbf{T}_{ij}^{-1}(\mathbf{k}_{ii}^{1})_m \mathbf{T}_{ij}, \quad (\mathbf{K}_{ij})_m = \mathbf{T}_{ij}^{-1}(\mathbf{k}_{ij})_m \mathbf{T}_{ij}, \quad (\mathbf{K}_{ji})_m = \mathbf{T}_{ij}^{-1}(\mathbf{k}_{ji})_m \mathbf{T}_{ij}, \quad (\mathbf{K}_{jj}^{1})_m = \mathbf{T}_{ij}^{-1}(\mathbf{k}_{jj}^{1})_m \mathbf{T}_{ij}. \quad \textbf{(10a–d)}$$

3. FORMULATION

Analysis of a space frame structure can be conducted by following a computer-oriented procedure outlined here. First, the 6 × 6 global stiffness submatrices in terms of the reference coordinates $\{x, y, z\}$ are generated for each member in the structure (e.g., member "i, j" shown in Fig. 3) using Eqs. (10a–d). Member "i, j" contributes to the stiffness matrices of nodes i and j at the ends of the member. Hence, corresponding elements from the global stiffness submatrices for this member may be transferred to the overall stiffness matrix by use of suitable indices (e.g., Weaver and Gere, 1990). The six possible displacements at a particular node i are denoted by the following indices:

$6(i - 1) + 1$ = index for the x component of translation,
$6(i - 1) + 2$ = index for the y component of translation,
$6(i - 1) + 3$ = index for the z component of translation,

$6(i-1)+4$ = index for the x component of rotation,
$6(i-1)+5$ = index for the y component of rotation,
$6(i-1)+6$ = index for the z component of rotation.

The transferring rule is that element (i_1, j_1) $(i_1, j_1 \in \{1, 2, \cdots, 6\})$ of submatrices $\left(\mathbf{K}_{ii}^{J}\right)_m$, $\left(\mathbf{K}_{ij}\right)_m$, $\left(\mathbf{K}_{ji}\right)_m$ and $\left(\mathbf{K}_{jj}^{I}\right)_m$ is added, respectively, to locations $(6i-6+i_1, 6i-6+j_1)$, $(6i-6+i_1, 6j-6+j_1)$, $(6j-6+i_1, 6i-6+j_1)$, $(6j-6+i_1, 6j-6+j_1)$ in the initial structure stiffness matrix $\mathbf{K}_I$. Construction of the complete $\mathbf{K}_I$ involves forming and transferring $\left(\mathbf{K}_{ii}^{J}\right)_m$, $\left(\mathbf{K}_{ij}\right)_m$, $\left(\mathbf{K}_{ji}\right)_m$ and $\left(\mathbf{K}_{jj}^{I}\right)_m$ for all members of the structure.

The second phase of the analysis is to generate initial load vectors. As shown in Fig. 3, the actions applied at node i, $(\mathbf{P}_I)_1$, $(\mathbf{P}_I)_2$ and $(\mathbf{P}_I)_3$, are the x, y and z components of the concentrated forces, and the actions $(\mathbf{P}_I)_4$, $(\mathbf{P}_I)_5$ and $(\mathbf{P}_I)_6$ are the x, y and z components of the moments applied at node i. They are put, respectively, at the locations $(6i-5)$, $(6i-4)$, $(6i-3)$, $(6i-2)$, $(6i-1)$ and $(6i)$ in the initial load vector.

After the construction of the required matrices is completed, substituting them into Eqs. (7) and (8) finally gives, with the boundary conditions enforced, the solution for free nodal displacements.

3.1 Mode I Loading

The tetrakaidecahedral unit cell under Mode I loading is shown in Fig. 4, with all of its members and joints numbered. All of the members (struts) of the cell have the same length L and cross-sectional area A. In addition, the following relations can be identified (Li and Gao, 2003):

$$A = \frac{2\sqrt{2}}{3} RL^2, \quad I_y = I_z = cA^2, \quad J = c_1 A^2, \tag{11}$$

where R is the relative foam density, and c and c_1 are two geometric constants depending on the strut cross section shape.

By following the procedure outlined above and using the structural and loading data illustrated in Fig. 4, the nodal displacements for each non-restrained joint of the cellular structure can be obtained. The effective Young's modulus, E_y^*, of the unit cell, and thus of the foam, can then be determined, using the average strain theorem in the homogenization theory (e.g., Gao et al., 2003), as (Li and Gao, 2003)

$$E_y^* = \frac{2\sqrt{2}P}{L\Delta_y}, \tag{12}$$

where Δ_y [$= (\Delta_1)_2$] is the displacement of the unit cell in the negative-y direction. From Eqs. (9a–d) and (11) it follows that that Δ_y, and thus E_y^*, depends on the relative foam density (R), the size and shape of the strut cross section (c, c_1, k_y and k_z), and the elastic properties of the strut material (E and G).

The effective Poisson's ratio ν_{xy}^* can be obtained as (Gao and Li, 2002; Li and Gao, 2003)

$$\nu_{xy}^* = -\frac{\sqrt{2}}{8}\frac{L}{\Delta_y}\sum_i \frac{(\Delta_i)_1}{x(i)}, \tag{13}$$

where $(\Delta_i)_1$ stands for the x-component of the (translational) displacement at node i, and $x(i)$ denotes the x-coordinate of node i. Clearly, $\nu_{zy}^* = \nu_{xy}^*$ due to symmetry.

Finally, the effective shear modulus G_{xy}^* can be shown to be (Li and Gao, 2003)

$$G_{xy}^* = \frac{9\sqrt{2}P}{8L\left(\Delta_{ys} - \Delta_{xs}\right)}, \tag{14}$$

where Δ_{xs} and Δ_{ys} are, respectively, the displacements of the cell in the x_s- and y_s-directions, which are oriented 45° relative to x- and y-axes (see Fig. 5).

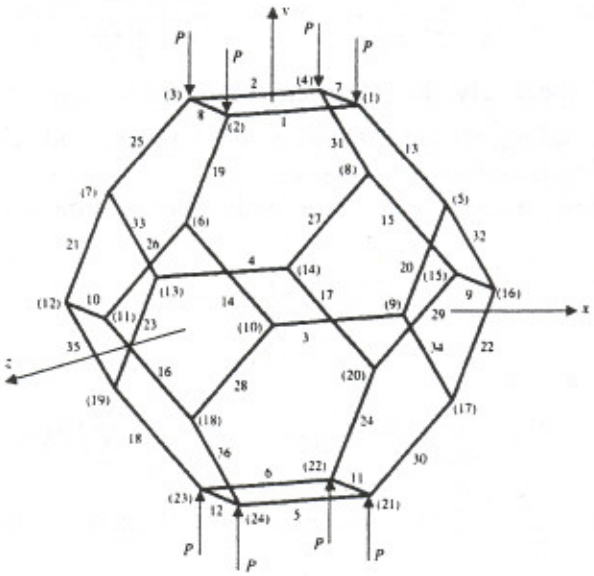

Fig. 4. Tetrakaidecahedral unit cell under Mode I loading.

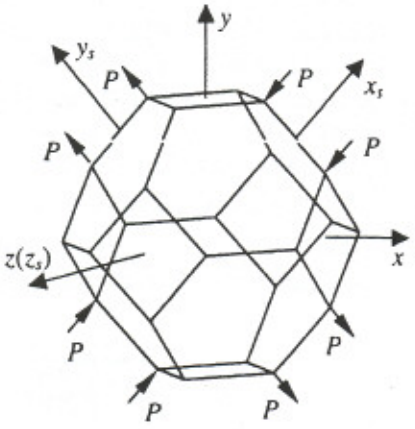

Fig. 5. Equivalent loading configuration for shear modulus (Mode I loading).

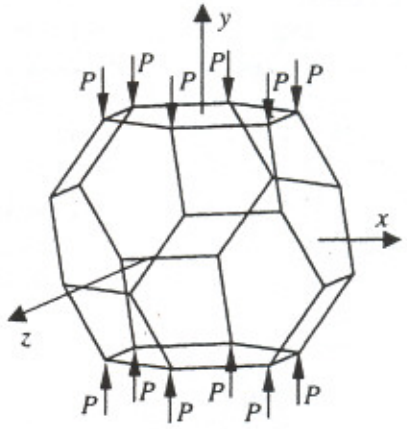

Fig. 6. Configuration for Young's modulus and Poisson's ratios (Mode II loading).

3.2 Mode II and Mode III Loading

Formulas for predicting the effective foam properties in the Modes II and III loading cases can be derived by following procedures similar to that used above for the Mode I loading case.

For the Mode II loading case (Fig. 6), the effective Young's modulus is obtained as (Li and Gao, 2003)

$$E_y^* = \frac{9\sqrt{2}P}{4L\Delta_y^{II}}, \tag{15}$$

and the effective Poisson's ratios as

$$\nu_{xy}^{*} = -\frac{\sqrt{6}}{20}\frac{L}{\Delta_y^{II}}\sum_i \frac{(\Delta_1)_1}{x(i)}, \quad \nu_{zy}^{*} = -\frac{\sqrt{6}}{24}\frac{L}{\Delta_z^{II}}\sum_i \frac{(\Delta_1)_3}{z(i)}, \tag{16a,b}$$

where Δ_y^{II} and Δ_z^{II} are, respectively, the displacements in the loading and lateral directions of the unit cell under Mode II loading, $z(i)$ denotes the z-coordinate of node i, and $(\Delta_1)_3$ stands for the z-component of the (translational) displacement at node i.

For the Mode III loading case (Fig. 2c), the effective Young's modulus is obtained as (Li and Gao, 2003)

$$E_y^{*} = \frac{5\sqrt{2}P}{8L\Delta_y^{III}}, \tag{17}$$

and the effective Poisson's ratios as

$$\nu_{xy}^{*} = -\frac{\sqrt{10}}{22}\frac{L}{\Delta_y^{III}}\sum_i \frac{(\Delta_1)_1}{x(i)}, \quad \nu_{zy}^{*} = -\frac{\sqrt{10}}{16}\frac{L}{\Delta_z^{III}}\sum_i \frac{(\Delta_1)_3}{z(i)}, \tag{18a,b}$$

where Δ_y^{III} and Δ_z^{III} are, respectively, the displacements in the loading and lateral directions of the unit cell under Mode III loading.

4. NUMERICAL RESULTS

To illustrate the new model, a parametric study of sample cases is conducted here for three-dimensional open-cell carbon foams, whose modeling motivated the present study. The MATLAB program (of The Mathworks, Inc.) is used in the computations. Young's modulus (E) and Poisson's ratio (ν) of the carbon strut material, which is assumed as isotropic, are, respectively, taken to be 15.61 GPa and 0.33, and the maximum value of the relative foam density (R) to be 0.22, as was done in Li et al. (2003). The shapes used here for the strut cross section also include circle, square, equilateral triangle and Plateau border.

The predicted effective Young's modulus (E_y^{*}), Poisson's ratio (ν_{xy}^{*}) and shear modulus (G_{xy}^{*}) varying with the relative density (R) for carbon foams with Plateau border strut cross sections and under Mode I loading are illustrated in Figs. 7, 8 and 9, where they are also compared to the predictions of several existing models.

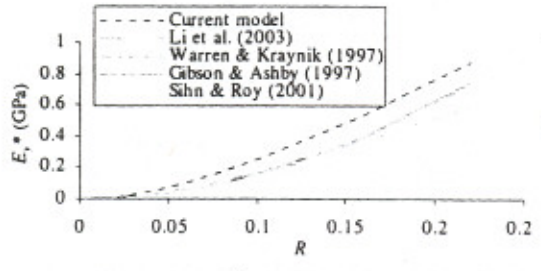

Fig. 7. Young's modulus vs. relative density.

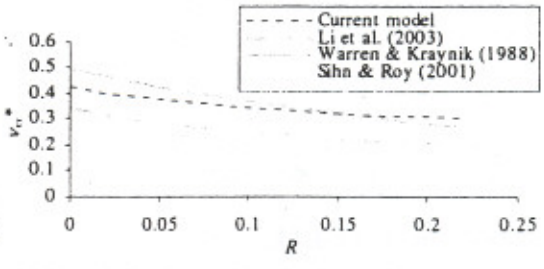

Fig. 8. Poisson's ratio vs. relative density.

From Fig. 7 it is seen that the values of E_y^{*} predicted by the current model and those by the four earlier models are very close for low-density foams (with $R < 0.1$). Figure 8 shows that ν_{xy}^{*} decreases monotonically as R increases according to the new model. This trend is the same as that predicted by three other models. Also, values of ν_{xy}^{*} predicted by the current model (e.g., $\nu_{xy}^{*} = 0.346$ at $R = 0.1$) are

close to 1/3, which is a value suggested by Gibson and Ashby (1997) based on available experimental data (ranging from 0.15 to 0.4).

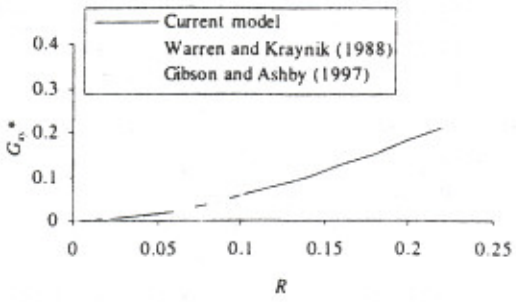

Fig. 9. Shear modulus vs. relative density.

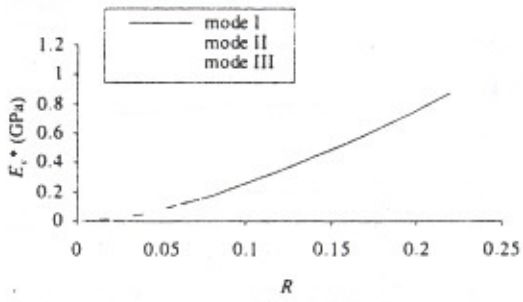

Fig. 10. Young's modulus vs. relative density.

It is clear from Fig. 9 that the values of G_{xy}^* predicted by the current model are closer to those provided by Gibson and Ashby (1997) based on the experimental data than the values given in Warren and Kraynik (1988). Moreover, Fig. 9 reveals that the predictions of G_{xy}^* by the three models are very close for low-density foams (with $R < 0.1$).

Figure 10 compares the predicted values of the effective Young's modulus (E_y^*) of carbon foams with Plateau border strut cross sections when the unit cell is under Modes I, II or III loading. It is shown that E_y^* increases monotonically for all the three loading cases as R rises. The values of E_y^* for the Mode I and II loading cases are very close for low-density foams (with $R < 0.15$), which conforms to the weak-anisotropy observed by Warren and Kraynik (1997). In this same low-density region, however, the values of E_y^* for the mode III loading case are 50% lower than those for the other two loading cases. This reflects the degree of anisotropy of carbon foams as measured by E_y^*.

For the tetrakaidecahedral unit cell under Modes I, II or III loading, the predicted values of the effective Poisson's ratios varying with R are illustrated in Figs. 11 and 12. For the Mode II loading case, ν_{xy}^* is 0.627 at $R = 0$ and decreases gradually with the increase of R, while ν_{zy}^* starts to descend from 0.212. When the unit cell is loaded at two farthest joints (Mode III loading), the values of both ν_{xy}^* and ν_{zy}^* are very close to those for the Mode II loading case. However, there are large differences between ν_{xy}^* and ν_{zy}^* for the same loading case. Furthermore, Figs. 11 and 12 show that for ν_{xy}^* or ν_{zy}^* the differences between the values for the Mode I loading case and those for the Modes II and III loading cases are significant. This indicates that carbon foams do exhibit distinct anisotropy when viewed in terms of Poisson's ratios. Also, it is observed from Fig. 12 that the predicted values of ν_{zy}^* for all of the three loading cases fall within the range of 0.15 - 0.4, which is the experimental data range quoted in Gibson and Ashby (1997).

The predicted effects of the relative foam density (R) on the effective shear moduli (G_{xy}^* and G_{zy}^*) are illustrated in Figs. 13 and 14. It is clear that the values of shear moduli are very close for all the three different loading cases. This agrees with the similarity between the results of the effective shear moduli for the Modes I and II loading cases reported in Warren and Kraynik (1997). In addition, it is noticed that the differences between the values of G_{xy}^* and G_{zy}^* under the same mode of loading are indistinguishable. These imply that the anisotropy as measured by the shear moduli is insignificant.

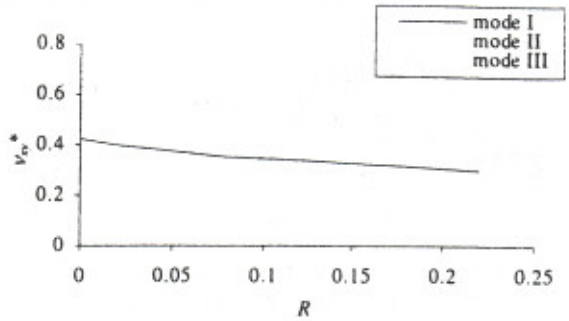

Fig. 11. Poisson's ratio vs. relative density.

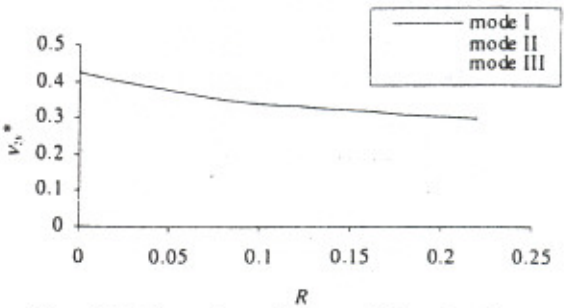

Fig. 12. Poisson's ratio vs. relative density.

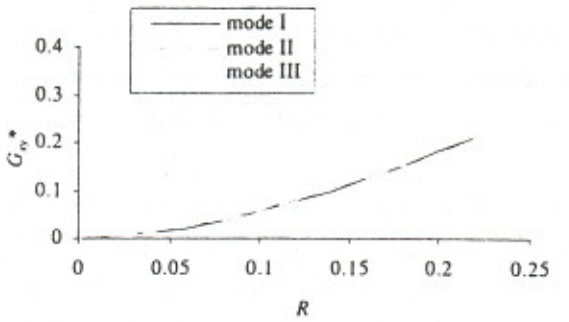

Fig. 13. Shear modulus vs. relative density.

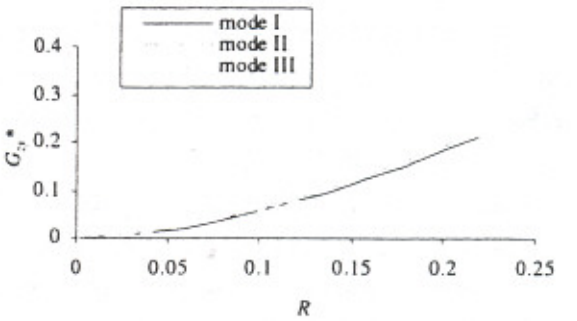

Fig. 14. Shear modulus vs. relative density.

Finally, the order of influence of strut cross section shapes on the effective properties of carbon foams appears to be the same in all three loading cases. That is, Plateau border, equilateral triangle, square and circle strut cross sections form a descending order for E_y^*, G_{xy}^* and G_{zy}^*, and a ascending order for both ν_{xy}^* and ν_{zy}^*. At $R = 0.1$, the maximum relative differences of the three elastic moduli and two Poisson's ratios, resulting from the use of different shapes of strut cross section, for the three loading cases are summarized in Table 1. In all of the three loading cases, shear moduli are most sensitive to the strut cross section shape, which is followed by Young's modulus and Poisson's ratios. It is noted from Table 1 that the values of relative differences between different loading cases are very close for all five elastic properties except for Poisson's ratios in the Mode III loading case, which are substantially lower than those in the Modes I and II loading cases. This supplements the observations about anisotropy in foam elastic behavior drawn from Figs. 11 and 12.

Table 1 Maximum relative differences due to the use of different strut cross section shapes

	Mode I	Mode II	Mode III
E_y^*	31.47%	33.02%	32.25%
ν_{xy}^*	8.93%	8.10%	1.30%
ν_{zy}^*	8.93%	7.25%	4.90%
G_{xy}^*	34.05%	33.63%	32.88%
G_{zy}^*	34.05%	33.50%	32.01%

ACKNOWLEDGEMENTS

The work reported here is partially funded by a grant from the AFOSR (Grant # F49620-03-1-0004). This support is gratefully acknowledged. The graduate assistantship and fellowship provided to Ke Li by Michigan Technological University are also greatly appreciated.

REFERENCES

Anderson, D. P., Kearns, K. M., Klett, J. W. and Roy, A. K., 2000, Microcellular graphite carbon foams for next generation structures and thermal management, in *Proc. the 2000 IEEE Aerospace Conf.*, Vol. 4, March 18-25, 2000, Big Sky, MT, pp. 193-199.

Balfour, J. A. D., 1986, *Computer Analysis of Structural Frameworks*, Nichols Publishing Company, New York, NY.

Gao, X.-L. and Li, K., 2002, Damaged mosaic laminate model of woven fabric composites with transverse yarn cracking and interface debonding, *Compos. Sci. Tech.* **62**, 1821-1834.

Gao, X.-L., Li, K. and Mall, S., 2003, A mechanics-of-materials model for predicting Young's modulus of damaged woven fabric composites involving three damage modes, *Int. J. Solids Struct.* **40**, 981-999.

Gibson, L. J. and Ashby, M. F., 1997, *Cellular Solids: Structures and Properties*, 2nd edition, Cambridge University Press, Cambridge.

Hall, R. B. and Hager, J. W., 1996, Performance limits for stiffness-critical graphitic foam structures. Part I: Comparisons with high-modulus foams, refractory alloys and graphite-epoxy composites, *J. Compos. Mater.* **30**, 1922-1937.

Li, K. and Gao, X.-L., 2003, manuscript to be published.

Li, K., Gao, X.-L., Roy, A. K., 2003, Micromechanics model for three-dimensional open-cell foams using a tetrakaidecahedral unit cell and Castigliano's second theorem, *Compos. Sci. Tech.*, (in press).

Roy, A. K., Pullman, D. and Kearns, K. M., 1998, Experimental methods for measuring tensile and shear stiffness and strength of graphitic foam, in *Proc. the 43rd Int. SAMPE Symp. and Exhibition*, May 31-June 4, 1998, Anaheim, CA, pp. 774-780.

Sihn, S. and Roy, A. K., 2001, Modeling and stress analysis of open-cell carbon foam, manuscript to be published.

Spillers, W. R., 1972, *Automated Structural Analysis: An Introduction*, Pergamon, Elmsford, NY, pp. 62-65.

Warren, W. E. and Kraynik, A. M., 1988, The linear elastic properties of open-cell foams, *ASME J. Appl. Mech.* **55**, 341-346.

Warren, W. E. and Kraynik, A. M., 1997, The linear elastic behavior of a low-density Kelvin foam with open cells, *ASME J. Appl. Mech.* **64**, 787-795.

Weaire, D. and Fortes, M. A., 1994, Stress and strain in liquid and solid foams, *Adv. in Phys.* **43**, 685-738.

Weaver, W. Jr. and Gere J. M., 1990, *Matrix Analysis of Framed Structures*, 3rd edition, Van Nostrand Reinhold, New York, NY.